Original scientific paper

Removal of nickel from Ni(II)-NH₃-SO₂-CO₂-H₂O system by electrocoagulation, sedimentation and filtration processes

Armando Rojas Vargas[1,2,✉], María Elena Magaña Haynes[3], Crispin Sánchez Guillen[3]
Forat Yasir Aljaberi[4,✉]

[1]Empresa de Servicios Técnicos de Computación, Comunicaciones y Electrónica "Rafael Fausto Orejón Forment", Holguín, Cuba

[2]Universidad de Holguín "Oscar Lucero Moya", Holguín, Cuba

[3]Centro de Investigaciones del Níquel "Alberto Fernández Monte de Oca", Holguín, Cuba

[4]Chemical Engineering Department, Chemical Engineering Department, College of Engineering, Al-Muthanna University, Al-Muthanna, Iraq

Corresponding authors: ✉arojas@eros.moa.minem.cu; ✉furat_yasir@yahoo.com

Abstract

The nickel removal by electrocoagulation of Ni(II)-NH₃-CO₂-SO₂-H₂O system was studied in a batch reactor of 50 L useful volume, with stirring and two pairs of aluminum electrodes. The operating parameters were nickel concentration between 255 and 342 mg L^{-1}, current density of 11.0 and 16.6 mA cm^{-2}, pH 8.34±0.06, mean temperature 58.4±3.9 °C and retention time of 50 min. The maximum nickel removal was 99.7 % at 11.0 mA cm^{-2}, specific energy consumption 16.86 kWh kg^{-1} of Al^{3+}, 2.438 kWh kg^{-1} of Ni and the adsorption capacity 5819 mg Ni g^{-1} of Al^{3+}. The precipitate contained a nickel content of 37.2 % and a true density of 2720 kg m^{-3}, hydrotalcite-like structure layered double hydroxides. The unit area of sedimentation was between 0.25 and 1.96 m^2 t^{-1} day, at a density from 971 to 1019 kg m^{-1} and 53±4 °C. A model for predicting the specific cake resistance was estimated as a function of pressure drop and suspension concentration at 44.45 kPa and 59.52 kg m^{-3}, resulting in the value of 6.47±107 m kg^{-1}. The average cake humidity was 88 % base humid.

Keywords

Electrocoagulation, kinetics, nickel removal, layered double hydroxide

Introduction

In ammoniacal carbonate leaching technology for the selective extraction of nickel and cobalt from the lateritic ore in Punta-Gorda, Cuba, a liquid effluent in the distillation process is obtained with several species in the solution of Ni(II)-NH₃-CO₂-SO₂-H₂O system [1]. The concentration of nickel (Ni^{2+}) is between 128 and 1000 mg L^{-1}, ammonia (NH_3) 120 - 920 mg L^{-1}, sulfur (S) 1.23-3.54 g L^{-1}, anions thiosulfate ($S_2O_3^{2-}$) 1.18-3.85 g L^{-1} and sulfate (SO_4^{2-}) 2.90-4.90 g L^{-1}. Furthermore, in this liquid effluent, the turbidity is smaller than 20 NTU, the colour is from 15 to 100 Pt/Co, the total hardness

60 - 115 mg L^{-1}, pH 7.38 - 8.62 and the flowed effluent reaches a temperature between 70 and 85 °C [2-5]. In a previous study, the possibility of removing dissolved nickel from this effluent by electrocoagulation (CE) was evaluated [6].

Electrocoagulation is an effective process for removing dissolved heavy metals presented in wastewaters of different industries. It is based on the destabilization of suspended, emulsified, or dissolved compounds in an electrolytic cell. The electric current flowing through the electrodes provides the electromotive force that causes a series of chemical reactions, resulting in the stability of polluting molecules. These molecules move through the applied electric field to form ionized components, electrolyzed, hydrolyzed, or free radicals being hydrophobic that adhere to the walls of the electrode, precipitate, or float, facilitating their removal by some secondary separation method [6-9].

The main parameters from the operating point of view are pH, current density (j), retention time (t) and temperature (T). To increase conductivity and energy efficiency, electrolytes such as Na_2SO_4, K_2SO_4 and NaCl have been fed. For nickel removal, an efficiency between 93 and 100 % has already been reported [6,9-12].

Vargas *et al.* [6] investigated the nickel removal from the $Ni(II)-NH_3-CO_2-SO_2-H_2O$ system by electrocoagulation. Using a complete experimental design and optimizing a multi-response procedure, the most favorable conditions of 95 % efficiency were obtained at 9.8 mA cm^{-2}, 60 °C, pH 8.65 and 40 min of electrolysis. Then, the investigation was carried out on a bench scale in a reactor with 25 L of useful capacity and a concentration of dissolved nickel between 300 and 562 mg L^{-1} [12]. The process efficiency was found between 97.7 and 99.7 %, at a specific energy consumption between 1.709 and 2.342 kWh kg^{-1} of Al^{3+}, or 0.7436 and 1.4007 kWh kg^{-1} of Ni, and adsorption capacity 3342 to 7264 mg Ni g^{-1} of Al^{3+} [12].

Thickening is the process of separating parts of the liquid of a suspension in such a way as to obtain a denser product and a flow of pure liquid. The objective of the process may be focused on obtaining a thicker pulp, or on recovering the liquid of a suspension. The first case is referred to as thickening and the second as clarification. The mechanism of thickening is sedimentation under the force of gravity. The best-known methods for sizing industrial settler tanks are Coe and Clevenger´s method [13], Kynch theory of batch sedimentation [14], Talmage and Fitch´s method [15], and Wilhelm and Naide´s method [16].

According to Stokes' law, particle size, the density difference between the dispersed phase and dispersion media, and fluid viscosity are the primary factors to consider in a sedimentation process. However, particle concentration, shape, surface charge and rheological properties of non-Newtonian fluids can also have a significant influence [17-20].

As the initial suspension concentration increases, the settling velocity becomes reduced due to an increase in collisions and interferences between particles [14,17,18]. Also, the settling velocity of discrete particles and sludges increases with increasing temperature due to the decrease in kinematic viscosity under the given sediment concentration [19,20]. The influence of temperature differentials in the settling tank may produce short-circuiting, cooler influent produces a bottom density current, while in the cases of a warmer influent, the density current is along the surface. In both cases, there is an increase in the concentration of suspended solids [20].

In regards to filtration, it is the unit operation in which a mixture of solid - liquid (suspension or slurry) or solid - gas is forced through a porous medium in which the solids are entrapped. The filtration experiments include the determination of the specific cake resistance to filtration and filter

medium resistance. The specific resistance is always used as a measure of the difficulty of fluid permeation through the filter [21-24].

An increase in suspension concentration at the filter inlet causes a decrease in the specific resistance and results in the reduction of energy consumption. Otherwise, when filtering suspension with low initial concentrations is fed, the ability of fine particles to migrate into the filter medium is greater and reduces fluid flow rates through them [21-23].

Pressure drop provides the driving force, in which slurry will be pressurized to flow through the filter medium. As pressure drop across the cake increase, the specific resistance augments as a power-law relationship [23,24]. An increase in the filtration pressure causes an increase in filtration flux, the filtration velocity, and at the same time results in reduction of cake porosity on the surface of the filter medium. The reduction in the porosity is caused by greater compression forces and results in an increase in the specific resistance, but for the larger size of a particle, more porous voids are presented in the cake layer [21,24].

The purpose of this research was to evaluate the electrocoagulation electric parameters, *i.e.,* specific energy consumption and current density for the nickel removal from the aqueous dissolution of the Ni(II)-NH$_3$-CO$_2$-SO$_2$-H$_2$O industrial system in a batch reactor, and to determine for the secondary separation the unitary area of sedimentation, the specific cake resistance and filtrate humidity.

Experimental

Electrocoagulation reactor

The electrocoagulation process was made in a complete mixed batch reactor. The body is metallic and cylindrical in shape with a plain base, diameter (D = 400 mm) and useful volume (V = 50 L) (Figure 1a).
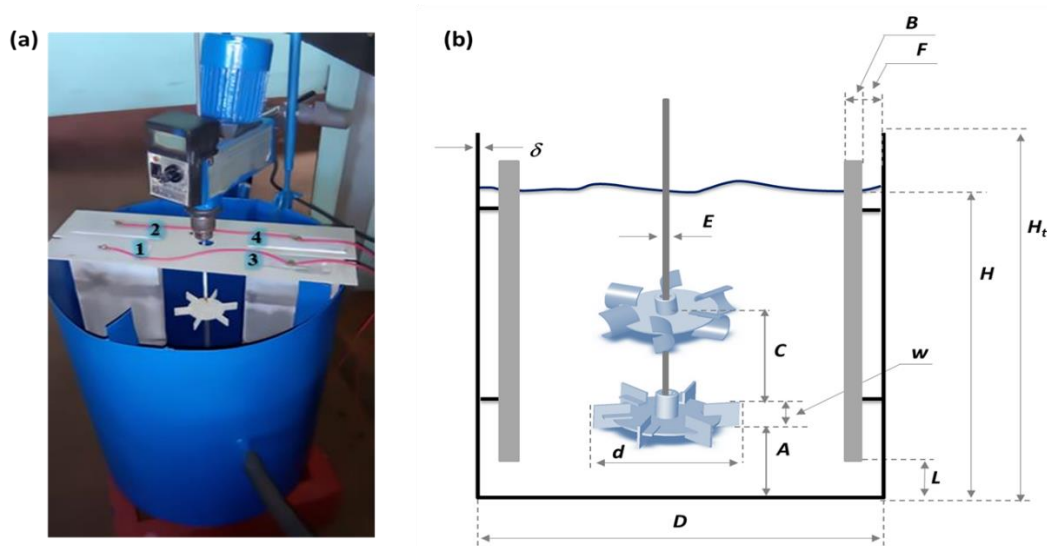

Figure 1. (a) Reactor of electrocoagulation; (b) factors of form

The reactor was equipped with a dual impeller mounted on the same shaft axis, comprised of six-bladed Rushton turbines (TR) and six concave-bladed disc turbines (CD-6). The separation distance between the impellers (C) was 200 mm and the rotating speed at 100 rpm. The factors of form were designed at standard conditions, as for impellent diameter (d), baffles wide (B), palettes wide (w) and impellent–base separation (A) according to the ratio: D/d = 3, H/d = 3, B/D = 0.1, w/d = 0.2,

A/d = 1. The baffle − reactor separation (*F/D*) was 1/50, and baffle–base separation *L/D* = 1/10 (Figure 1b) [12].

Also, the reactor was prepared with 2 couples of electrodes, wide 125 mm, long 190 mm, useful area of 0.095 m^2, 8 mm distance between electrodes and the following chemical composition: 98.98 % Al, 0.5 % Mg, 0.33 % Fe and 0.114 % Si.

A direct current (DC) power supply BCA-5KT was used with the characteristics: input voltage 220 V, output voltage 0 to 150 V and output current 0 to 20 A. The electric parameters were measured using a multimeter UNITE-T (UT-208) (Figure 2).
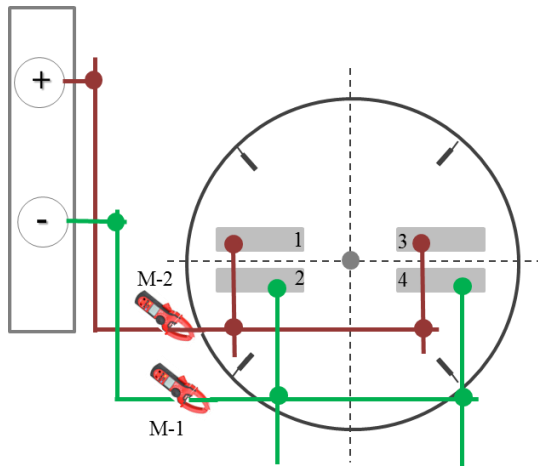

Figure 2. *Installation of electrodes (1 to 4), point to electric current measurement (M-1, M-2), and voltage between (1-2) and (3-4)*

Operation parameters of electrocoagulation

The electrocoagulation parameters were determined considering the results of previous studies on a bank scale with 25 L of useful volume [12].

The consumption of aluminium electrode (W_E / g) was estimated starting from the initial nickel concentration (g L^{-1}), the adsorption capacity at equilibrium (Q_e / mg g^{-1}), and the useful volume of the reactor (*V* = 50 L). As for current intensity (*I* / A), using the Faraday's law, eq. (1), and the electric current efficiency (η), eq. (2), (see Figure 3) [6-12].
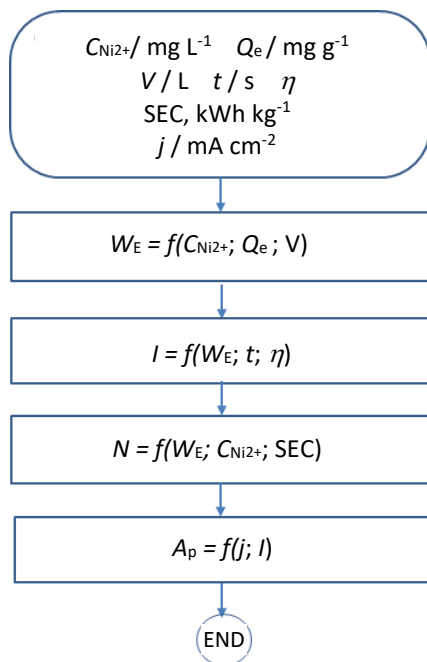

Figure 3. *Algorithm to scaling electrical parameters*

$$W_F = \frac{IMt}{ZF}$$

(1)

$$\eta = \frac{W_E}{W_F}$$

(2)

where $Z = 3$ is a number of electrons, molecular weight (M) for aluminum is 26.98 g mol^{-1}, the Faraday´s constant, $F = 96485.33$ C mol^{-1}, t / s is electrocoagulation time, and W_F / g) is the amount of Al dissolved according to Faraday's law.

The electric potency (N / kW) was selected at the maximum value with respect to the specific energy consumption (SEC, kWh kg^{-1}) for each initial nickel concentration evaluated. Regarding the effective area of electrodes (A_p), it was estimated starting from the current intensity (I / A) and the current density (j / mA cm^2).

The specific energy consumption (SEC) was calculated by Eq. (3):

$$SEC = \frac{ZFU}{3600 M \eta}$$

(3)

where U / V is electrical voltage and SEC, kWh kg^{-1} Al^{3+} is the specific energy consumption.

Consequently, the electrocoagulation experiments consisted of determining the nickel removal (X / %), the consumption of aluminium electrodes (W_E / g), the electric current efficiency (η), and the specific energy consumption (SEC), at an electric current intensity of 10 and 15 A, electrolysis time (t =50 min, pH 8.5±0.1 and temperature of 60 °C).

A sufficient quantity of suspension was produced through three experimental runs to make the sedimentation and filtration experiments. Synthetic liquor (S-1) and effluent liquor (E-2, E-3) were fed to the reactor. The synthetic liquor was prepared using basic nickel carbonate, ammonium hydroxide, sulfuric acid, and distilled water. The effluent liquor was sampled in the distillation columns discharge at the production plant in Punta-Gorda, Cuba (Table 1).

Table 1. Characterization of liquors fed to electrocoagulation

Liquor	Concentration, g L^{-1}			
	Ni	NH$_3$	CO$_2$	S
S-1	0.255	1.59	1.03	0.66
E-2	0.342	0.31	0.10	2.38
E-3	0.269	0.49	0.19	1.95

Nickel removing

The nickel removing (X / %) and the adsorption capacity (Q_t/mg g^{-1}) or amount of adsorbate adsorbed per adsorbent unit were determined by Eqs. (4) and (5):

$$X = 100x = 100 \frac{C_0 - C_t}{C_0}$$

(4)

$$Q_t = (C_0 - C_t) \frac{V}{W_F}$$

(5)

where x is the converted fraction, C_0 / mg L^{-1} is the initial concentration of nickel, C_t / mg L^{-1} is the concentration of nickel in the liquid phase in each time interval and V / L is the volume.

When the duration of the process is long enough, Q_t is constant and determines the charge or adsorption capacity (Q_e / mg L^{-1}) corresponding to the concentration at equilibrium (C_e / mg L^{-1}).

Kinetic model

Avrami's fractional kinetic model describes the change in volume (or mass) of a crystal as a function of crystallization time, although it has been assumed as an empirical model for the analysis of adsorption kinetic data. It is represented by differential eq. (6), integrated eq. (7) and linearized eq. (8) forms [25-28]:

$$\frac{dQ_t}{dt} = k_{av}^n t^{n-1} \left(Q_e - Q_t \right) \tag{6}$$

$$Q_t = Q_e \left(1 - e^{-(k_{av}t)^{n_{av}}} \right) \tag{7}$$

$$\ln \left[-\ln \left(1 - \frac{Q_t}{Q_e} \right) \right] = n_{av} \ln k_{av} + n_{av} \ln t \tag{8}$$

where, k_{av} / min^{-1} is the kinetic constant or global constant, n_{av} is the fractional reaction order, Q_e and Q_t are the amount (mg g^{-1}) adsorbed in the equilibrium and at time t from the start of the process, respectively.

The Elovich's model, which was firstly proposed by Roginsky and Zeldovich, can be expressed mathematically by Eq. (9) and assuming $\alpha \beta t \gg 1$, a linear form is obtained as eq. (10) [29-31]:

$$\frac{dQ_t}{dt} = \alpha\, e^{\beta Q_t} \tag{9}$$

$$Q_t = \frac{1}{\beta} \ln(\alpha\beta) + \frac{1}{\beta} \ln t \tag{10}$$

where, α (mg g^{-1} min^{-1}) is the initial adsorption rate, and β (g mg^{-1}) is a constant related to the extension of surface coverage.

Bangham's equation was used to evaluate adsorbate pore diffusion activities, if the adsorption is pore-diffusion controlled, eq. (11) [32,33].

$$\ln \left(\frac{c_0}{c_0 - Q_t \dfrac{W}{V}} \right) = \ln \left(\frac{k_B W}{V^2} \right) + \alpha \ln t \tag{11}$$

where, C_0 / mg L^{-1} is the initial concentration of nickel (adsorbate), W / g is the weight of the adsorbent, V / L is the volume of the solution, k_B / mL g^{-1}·L and $\alpha < 1$ are constants.

The Weber and Morris's model suggests that intra-particle diffusion is involved in the adsorption process, or two or more steps govern the adsorption process. However, if a linear graph is obtained and the plot passes through the origin, then intra-particle diffusion is said to be the sole rate-limiting step, Eqs. (12)-(13) [30,31]:

$$\frac{dQ_t}{dt} = \frac{1}{2} k_d t^{-0.5} \tag{12}$$

$$Q_t = k_d \sqrt{t} + c \tag{13}$$

Where k_d /mg g^{-1} min$^{-1/2}$ is the rate constant for intra-particle diffusion, c / mg g^{-1} is a constant associated with the thickness of the boundary layer (a higher value corresponds to a greater effect on the limiting boundary layer).

The conversion time model was proposed by Rojas-Vargas [12]. The model relates the conversion time (t) as a function of the converted fraction (x), the initial concentration (g L^{-1}) of nickel, sulfur, carbon dioxide and aluminum mass, Eqs. (14) and (15).

$$t = \left\{ a\left[1-(1-x)\right]^{\frac{1}{2}} + b\left[5\left[-\ln(1-x)\right]^{\frac{1}{5}}\right] + c\left[1-(1-x)^{\frac{1}{3}}\right] + d\left[x^{\frac{2}{3}}(1-x)^{\frac{2}{3}}\right] \right\} C_{Ni}{}^{e} C_{S}{}^{f} C_{CO_2}{}^{g} C_{Al}{}^{h}$$

(14)

where mechanisms coefficients are ascribed to: *a* - external diffusion resistance; *b* - nucleation; *c* - chemical reaction and *d* - autocatalytic effect by the Roginskii-Shultz equation. The constants *e, f, g* are the exponents of the initial concentration of nickel, sulfur and carbon dioxide, respectively.

The Faraday low was used to determine the aluminum mass and transformation of eq. (14) results in eq. (15):

$$t^{n} = \left\{ a\left[1-(1-x)\right]^{\frac{1}{2}} + b\left[5\left[-\ln(1-x)\right]^{\frac{1}{5}}\right] + c\left[1-(1-x)^{\frac{1}{3}}\right] + d\left[x^{\frac{2}{3}}(1-x)^{\frac{2}{3}}\right] \right\} C_{Ni}{}^{e} C_{S}{}^{f} C_{CO_2}{}^{g} K_{Al}$$

(15)

where, the coefficient K_{Al} depends on the electrical current fed to the process. The exponent of the conversion time (n) has a positive numerical value, it reflects the favorable effect and the high dependence that the process has on the formation of aluminum hydroxide, [Al(OH)$_3$], the main flocculating agent and formation of aggregates due to the high interfacial area.

Unitary area of sedimentation

The Talmadge-Fitch and Coe-Clevenger methods were used to obtain the unitary area of sedimentation at da ensity of the slurry (ρ_p) 971 - 1019 kg m^{-3} anda temperature 53±4 °C [13,15].

The Talmadge-Fitch geometric method of thickener design consist of drawing the tangent to the free-fall zone (r_1) and to the compression zone (r_2) in the settling curve; using the bisector (r_3) to the angle formed at the interception of (r_1) and (r_2) the critical point (pC) is obtained. Then, drawing the tangent (r_4) to the critical point perpendicular to (r_3) and the asymptote (r_5) to the depth *Hu* corresponding to the final concentration of the sludge, the thickening time (t_u) is obtained (Figure 4).
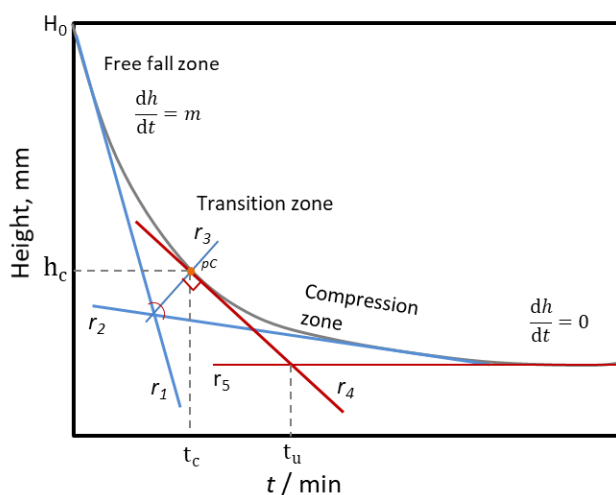

Figure 4. *Talmadge and Fitch thickener design method*

So, the free settling velocity (v_f / m h^{-1}), the critical settling velocity (v_c / m h^{-1}), and the unit area of sedimentation (*UA* / m^2 day t^{-1}) are calculated, Eqs. (16)-(18).

$$v_f = m = \frac{dh}{dt}$$

(16)

$$v_c = \frac{h_c}{t_c}$$

(17)

$$UA = \frac{10^5 t_u}{144 H_0 C_0}$$

(18)

where t_u / min is the thickening time required to reach a wanted concentration of sludge, H_0 / mm is the initial height of the pulp in the test tube, C_0 / kg m^{-3} is the initial concentration of solids.

On the other hand, the Coe-Clevenger method requires that pulps of various concentrations between the thickener feed and underflow be prepared. The method consists of determining the critical sedimentation time (t_c / min) and carrying out extractions of the supernatant liquor from the test tubes at the height (h_e / mm) corresponding to several predetermined volumes (200, 300... to 750 mL) at a critical time (t_c). Then the suspended solids concentration, the settling velocity (v_s / m·h^{-1}) and the unit area (*UA*) are calculated, Eqs. (19), (20).

$$UA = \frac{10^5 t_u}{144 H_0 C_0}$$

(19)

$$UA = \left\{ \left[\frac{L}{S}\right]_0 - \left[\frac{L}{S}\right]_f \right\} \frac{1000}{24 \rho_l v_s}$$

(20)

where, v_s / m h^{-1}) is the settling velocity, L / S (kg kg^{-1}) is the initial (0) and final (f) liquid-solid relationship, and ρ_l / kg m^{-3} is the liquid density.

Constant pressure filtration

The filtration tests were carried out by the constant pressure method [34].

The sludge specific resistance to filtration (α / m kg^{-1}), resistance (R_m / kg^{-1}) of filter medium and filtrate humidity (Y / %) ware determined. The sludge was prepared in volumes of 150, 200, 250, 300 and 400 mL and heated in a water bath at 60 °C. Before being poured into the Büchner funnel, it was shaken to avoid sedimentation influences.

The filtration pressure drop (ΔP) was 28.0 and 44.0 kPa and suspension concentration (C_s) 25.0 and 60.0 kg solid per m^3 pure liquid. The area (A_f) was 1.608×10^{-4} m^2. Filter paper for quantitative analysis, CHMLAB F1004, with pores size 0.02-0.025 mm, was used as a membrane.

The common model for constant pressure filtration is represented by eq. (21):

$$\frac{t}{V} = \frac{\mu \alpha C_t}{2 A_f^2 \Delta P} V + \frac{\mu}{A_f \Delta P} R_m$$

(21)

where μ / Pa s is the liquid viscosity, and C_t / kg solid per m^3 liquid filtrated is the concentration.

The synthesis product was dried in a vacuum oven at 60 °C during 74 h. The humidity was calculated base humid, eq. (22).

$$Y_h = \frac{m_h - m_d}{m_h}$$

(22)

where, m_h / g is the humid mass, m_d / g is the dry mass, and Y_h is the humidity base humid.

Chemical analysis

The chemical analyses were performed applying volumetric, gravimetric, potentiometric, atomic absorption spectrophotometry (AAS) and X-ray diffraction methods.

The pH measurements were performed at 25 °C, using a pH meter PHILIPS PW-9420, 115-230 V, 50–60 Hz, precision 0.001 pH / °C. Metals determinations were made using a Spectrophotometer SP-9. The electrode characterization was realized with a Spark optical emission spectrometer (OES) model GS 1000-II.

X-ray diffraction (XRD), X'PERT3 equipment, Cu anode lamp (CuKα radiation) and wavelength 0.15405 nm, constant scanning at a measurement interval of (2θ) between 4.0042 and 79.9962° with a step of 0.0080° measured every 5 min. The potential difference is 45 kV and the current 40 mA, calibration external with silicon standard. The qualitative analysis of phases was performed using the PANalytical HighScore program.

Results and discussion

Nickel removal by electrocoagulation

Electrocoagulation (EC) was carried out with synthetic liquor (S-1) and effluent liquor (E-2, E-3) of the industrial process. The nickel concentration was of 289±47 mg L^{-1}, ammonia 0.78±0.69 g L^{-1}, dioxide of carbon 0.44±0.51 g L^{-1}, sulfur 1.66±0.90 g L^{-1} and pH 8.34±0.06. The average operating temperature was 58.4±3.9 ºC (see Table 1).

The maximum nickel removal was 99.7 % (E-2) at an electric current of 10.5±2.6 A, but with synthetic liquor (E-1), it was 94.1 % at 10.4±0.6 A, which is due to the favorable effect of the ionic species in the effluent liquor of the industrial process, on the removal efficiency (Figure 5) [12].
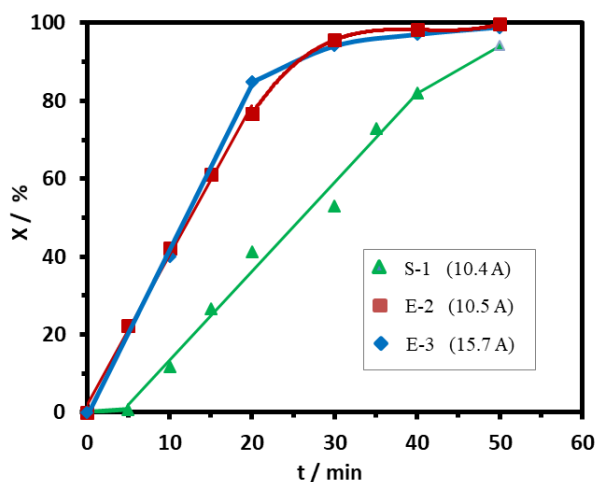

Figure 5. Nickel removal by electrocoagulation from liquor synthetic (S) and effluent (E)

Regarding the experiment (E-3) at 15.7±2.8 A, the nickel removal was 98.9 %, which suggest that the electric current of 10.5 A (11.0 mA cm^{-2}) is appropriate to the process. In agreement with Faraday's law, increasing the current electric leads to a higher Al^{3+}, OH$^-$ production, and electro-coagulant formation, but in turn, it increases operating costs and undesirable processes, such as heat generation and an excessive oxygen evolution reaction. In all the experiments, the formation of abundant foam around and between the electrodes was observed, suggesting a need for the evacuation and treatment of the foam in a continuous industrial system.

The behavior of the electric parameters

The electric current diminished slightly with the reaction time from 10.97 to 9.77 A and so, to correct this tendency, at 40 min, it was increased up to 11.5 A (Figure 6).

The voltage increased from 1.68 V to 2.0 V, and after 40 min to 2.56 V when the electric current was corrected (Figure 6 b). These trends in the electric parameters are due to the decrease of the

suspension conductivity directly proportional to the reduction in the nickel concentration and of the anions [$S_xO_y^{Z-}$] and [CO_3^{2-}] and also due to the increase of deposits on electrodes that growth the resistance to the passage of the electric current [9].

The increases in electric current with two pairs of electrodes of different areas, 0.06 m^2 and 0.0952 m^2, were evaluated (see Figure 7). The greater the area, the lower the voltage required to generate the operating current. This is due to the fact that when the electrode area (A_e) increases, the resistance (R) to the passage of electrons between the electrodes under the effect of electric field decreases, that is, the opposition to the charge flow decreases, eq. (23). According to Ohm's law, the voltage (U) decreases proportionally with the reduction of the resistance for a fixed value of the current flow (I) that circulates through the closed electrical circuit, eq. (24).
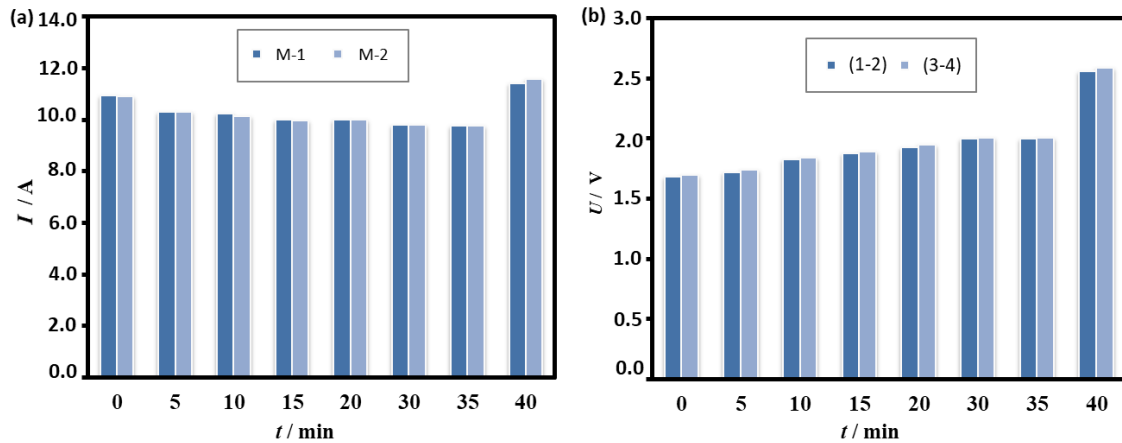

Figure 6. *(a) Electric current and (b) voltage during the electrocoagulation process (S-1), at 60 ℃ and 10.97 mA cm^{-2}, total useful area of electrodes 0.095 m^2*

$$R = \rho_e \frac{L}{A_e} \tag{23}$$

$$R = \frac{U}{I} \tag{24}$$

where, R / Ω is electric resistance, ρ_e /$\Omega \cdot m^{-1}$ is the resistivity of the at a given temperature, L is longitude of the driver, and A_e is area of the traverse section of the driver.
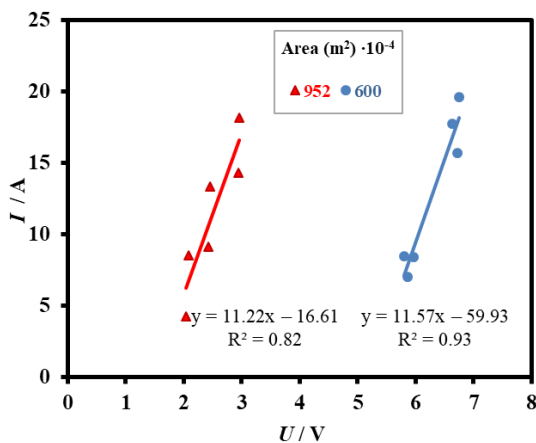

Figure 7. *Variation of the electric current versus voltage for different electrode areas (S-1)*

However, in the experiment with effluent liquor (E-2), greater resistance to the passage of electrons between the aluminum electrodes was observed from the initial minutes of electro-coagulation (Figure 8). Measurements on the M-1 side showed higher electrical current than on the

M-2 side, which may be associated with more intense electrolytic reactions at electrode surfaces, the nucleation and the growth of deposits (see Figure 2). The electric current that displayed the output of the power supply BCA-5KT remained approximately constant equal to 10.2±0.5 A, and equal to the average of the measurements in M-1 and M-2. In this experiment, the voltage was controlled at irregular intervals to avoid the electric current diminishing and resulting in 12.90±0.54 A (M-1) and 7.73±0.44 A (M-2).

Regarding the process carried out at 16.6 mA cm^{-2}, a similar trend in the electrical parameters was obtained as those represented in Figure 8. The measurements on the M-1 side obtained an average of 18.42±0.44 A while on the M-2 side of 13.06±0.44 A. The voltage was 7.07±0.53 V (1-2) and 7.08±0.52 V (3-4). On the other hand, the current output of the power supply remained approximately constant equal to 15.63±0.55 A.
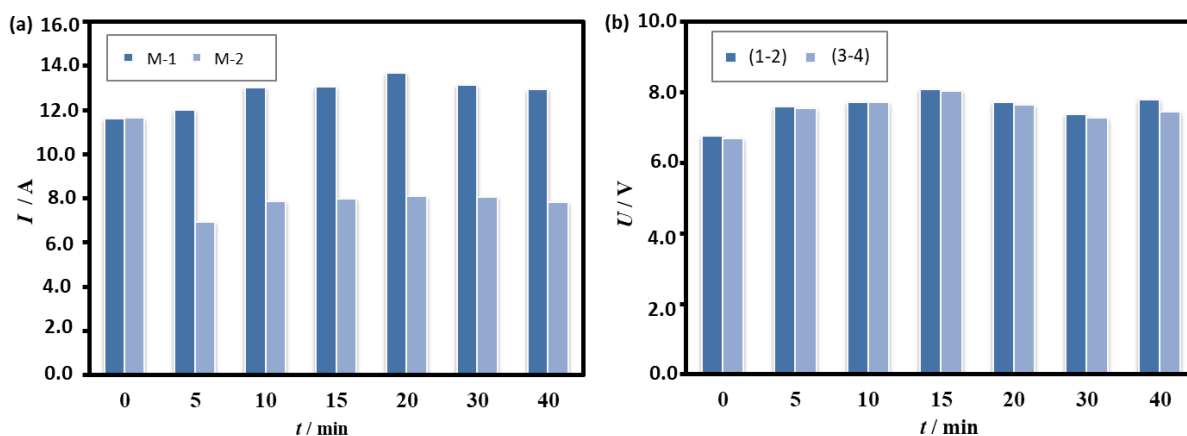

Figure 8. *(a) Electric current and (b) voltage during electrocoagulation process (E-2), at 60 °C and 11.03 mA cm^{-2}, total useful area of electrodes 0.095 m^2*

Implementing a polarity switching in which the current direction in the reactor is reversed at regular intervals, and the addition of aggressive ions decreases deposit formation and electrode passivation, increases the solution conductivity and, therefore, the resistance to the passage of electric current is lower [10]. On the other hand, solar photovoltaic energy is an environmentally friendly alternative and could reduce the operation cost of the electrocoagulation process [11,35].

Regarding the electric current efficiency (η), it was 130.5±4.9 %. The specific energy consumption was estimated for a remaining dissolved nickel concentration of 15 mg L^{-1}, resulting in 16.86 kWh per kg Al^{3+} and 2.44 kWh per kg Ni^{2+} for the experiment E-2. The adsorption capacity (Q_e) at the maximum removal efficiency was between 3022 and 4117 mg Ni per g Al^{3+} (Table 2).

Table 2. *Electric and equilibrium parameters*

Liquor	C_{Ni} / mg L^{-1}	j / mA cm^{-2}	C_e / mg L^{-1}	X / %	η / %	SEC, kWh kg^{-1}		Q_e / mg Ni per g Al
						Ni	Al	
S-1	255	11.0	15.0	94.1	130	1.46	4.60	4114
E-2	342	11.0	15.0	95.6	127	2.44	16.86	5918
E-3	269	16.6	15.0	97.0	134	4.40	16.82	3022

Kinetic analysis

Kinetic models were fitted in the order: Avrami > Bangham > Elovich. The best fit model was chosen by comparing the determination coefficients R^2 values (Table 3).

Avrami's fractional kinetic model better describes nickel removal by electrocoagulation. It refers to the nucleation, growth orientation of crystallites [36] and possible changes in the adsorption mechanism [32], *i.e.,* diffusion, surface interaction with random nucleation, or both [28].

Elovich's model assumes that the active sites of the adsorbent are heterogeneous and exhibit different activation energies. It also describes multiple reaction mechanisms such as adsorbate molecules transport in the solution phase (bulk diffusion) and the surface diffusion. In this last mechanism, the adsorbate molecules are transported from the bulk liquid phase to the adsorbent external surface through a hydrodynamic boundary film [31]. As the current density increases, the constants related to the rate of adsorption (α) and the surface coverage (β) also increase.

Bangham's model was suitably fitted and suggests the influence of external mass transfer followed by pore diffusion. On the other hand, the intra-particle diffusion model showed a linear graph (S-1), but the plot did not pass through the origin, the constant associated with the thickness of the boundary layer resulted in the negative ($c<0$) (S-1, E-2) and the determination coefficient R^2 was low (E-2, S-3), validating that adsorbate pore diffusion is not rate-controlling step [31,32].

***Table 3.** Kinetic model parameters*

Liquor	S-1	E-2	E-3
C_{Ni} / mg L^{-1}	255	342	269
j / mA cm^{-2}	11.0	11.0	16.6
Avrami			
k_{av} / min^{-1}	0.036	0.071	0.068
n_{av}	2.436	1.41	1.453
Q_e / mg g^{-1}	4117	5819	3022
R^2	95.10	99.04	97.30
Elovich			
α/ 10^{-2} mg·g^{-1}·min^{-1}	2.79	7.72	4.19
β/ 10^4 g mg^{-1}	5.48	4.65	9,07
R^2	93.25	97.26	93.38
Bangham			
k_B / mL g^{-1} L	1.19	20.16	16.27
α	2.34	1.40	1,316
R^2	96.85	99.04	95.49
Intra-particle diffusion			
k_d / 10^{-2} mg g^{-1} min$^{-1/2}$	8.78	9.80	4.33
C /10^{-2} mg g^{-1}	-2.14	-4.73	2.29
R^2	98.23	92.30	80.08

The conversion time kinetic model (CTV) presented the best quality of adjustment, as for the largest coefficient of determination R^2 of 99.31 % and adjusted R^2 of 98.99 % (Table 4).

***Table 4.** Parameters of the conversion time kinetic model (CTV), liquors S-1 and E-2, 11 mA cm^{-2}*

n[1]	a[2]	b[2]	c[4]	d[5]	e[6]	f[7]	g[8]	K_{Al}[9]
0.3138	0.6032	0.4091	1.1919	2.6276	0.2497	-0.7414	-0.2994	0.1422

[1]time constant; [2]extern diffusion; [3]nucleation; [4]chemical reaction; [5]autocatalysis; [6]Ni constant; [7]S constant; [8]CO$_2$ constant; [9]Al constant

CTV model suggests the simultaneous contribution of the resistance of the mechanisms: external diffusion (*a*), nucleation (*b*), the chemical reaction (*c*) and a possible autocatalytic effect (*d*). According to the model coefficients, the process is probably under the control of the chemical

reaction. The contaminants (S, CO_2) perform a favorable effect over the nickel removal. The oxy-sulfur ions [$S_xO_y^{z-}$] and carbonate [CO_3^{2-}] ions are attracted by electrostatic forces to balance charges and adsorbed on the active centers of the coordination surface; furthermore, those can be displaced by other competing ions in the solution (exchange adsorption) due to the interactions between the ions on the charged surface and in the diffuse layer around the surface, and the nickel removal by the formation of Ni-Al/LDH is promoted [12].

Synthesis product characterization

The synthesis product was characterized by atomic absorption spectrometry (AAS) and X-ray diffraction (XRD). The precipitate had a nickel concentration between 30.86 and 38.26 %, aluminum from 6.4 to 7.2 %, sulfur 6.19 to 6.36 %, as well as cobalt and magnesium in lower concentrations (Table 5).

The true density, defined as the quotient of mass over the volume of a sample without considering pores in the material, was from 2377 to 2720 kg m^{-3}. On the contrary, the apparent density that includes pores and water was 600-640 kg m^{-3}.

Table 5. *Characterization of the synthesized product*

Liquor	Concentration, wt.%					Density, kg m^{-3}	
	Ni	Co	Mg	Al	S	True	Apparent
S-1	38.26	0.689	0.136	6.4	6.36	2377	620
E-2	37.21	0.059	1.300	6.6	6.24	2720	640
E-3	30.86	0.062	1.390	7.2	6.19	2570	600

Regarding XRD analysis, the largest diffraction peaks were obtained at 2θ Bragg angles of 10.098±0.085, 22.005±0.085, 35.034±0.085 and 61.070±0.085°, which are assigned to the crystalline planes, according to the Miller indices (hkl): (003), (006), (012), (110) respectively, are also of interest at 72.220±0.12° (019). These diffraction peaks are indexed on a hexagonal system with rhombohedral symmetry, special group R-3m (polytype of three layers), hydrotalcite-like structure layered double hydroxides. The presence of 0kl peaks anticipates the presence of stacked layers (Figure 9) (JCPDS file 15-0087) [37-41].
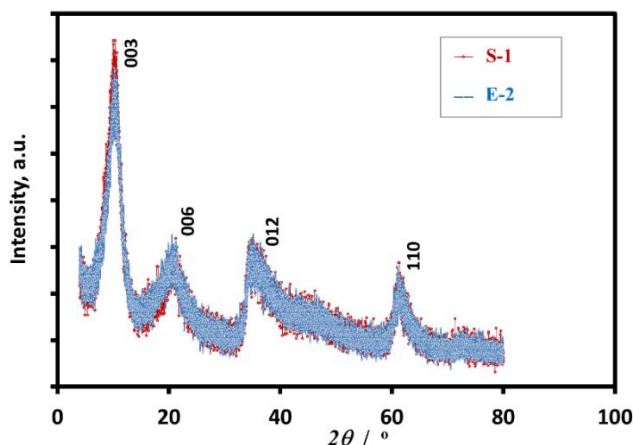

Figure 9. *X-ray diffraction (XRD) of the synthesized product*

The XRD pattern also showed phase impurities by comparison of the characteristic reflection pattern to a reference library of samples, such as nickel hydroxide-oxyhydroxide (Ni(OH)$_2$ NiOOH), nickel aluminum oxide hydrate (Ni$_5$Al$_4$O$_{11}$·18H$_2$O) and aluminum oxide hydrate (5Al$_2$O$_3$·H$_2$O).

From the XRD analysis, the spacing (d_{hkl}) of the LDHs, the crystal lattice parameters (a and c) and the crystallite size (D_{hkl}) were determined (Table 6).

Table 6. *Lattice parameters and size of Ni/Al-LDH crystallites*

Sample	Spacing, nm				Cell parameters, nm		V / nm^3	Crystallite size, nm	
	d_{003}	d_{006}	d_{012}	d_{110}	$a = b$	c		D	D_{003}
S-1	0.8853	0.4039	0.2561	0.1513	0.303	0.244	0.193	12.2	13.0
E-1	0.8693	0.4021	0.2556	0.1515	0.303	0.242	0.192	8.5	13.3

The separation of the planes (d_{hkl}) of the LDH, also called spacing, basal distance, or thickness of the interlayer gallery, was calculated using Bragg's law and is similar to the compounds synthesized by coprecipitation reported in the literature: [Ni/Al-SO$_4^{2-}$] ($0.801 \leq d_{003} \leq 0.859$ nm) and [Ni/Al-NO$_3^{-}$] ($0.782 \leq d_{003} \leq 0.876$ nm) [42,43,44] and [Ni/Al-CO$_3^{2-}$] ($0.740 \leq d_{003} \leq 0.763$ nm) [38]. The variation in the basal distance is due to the variation in the amount (intercalation degree) and type of anions (atom size and valence) in the LDH interlayer.

Parameters a and c were calculated using the relationship between the spacing (d_{hkl}) in the planes (hkl): (003), (006), (012), (110) and the lattice parameters (a, b and c) for the hexagonal crystal system ($b = c$). The data were adjusted using the Statgraphic Centurion XVII software in the nonlinear regression option. The average values of the lattice parameters ($\pm$ standard deviation) were: $\underline{a}$ = b = 0.303 nm and c equal to 0.243 ± 0.014 nm, with a fit quality greater than 99.9 %, confirming that it is a hexagonal crystalline system. The parameter a is equivalent to the average distance between the center of adjacent cations in the lattice, and c is the basal axis, which is related to the distance between neighboring atoms and the interlayer distance.

The parameters have been reported for the compounds obtained by coprecipitation: [Ni/Al-SO$_4^{2-}$]-LDH values of a = 0.303 nm and c = 0.2405 nm; and for [Ni/Al-CO$_3^{2-}$]-LDH in the following ranges: $0.302 \leq a \leq 0.308$ nm and $0.222 \leq c \leq 0.2405$ nm [8,41,43,44].

The unit cell volume ($V = 0.866\ a^2c$) was 0.192 ± 0.0007 nm^3, similar to other [CO$_3^{2-}$]-LDH obtained by co-precipitation such as [Zn/Al] 0.189 nm^3, [Ni/Al] 0.1876 nm^3 and [Mg/Al] 0.180 nm^3. On the other hand, by the sol-gel method it was lower [Ni/Al] 0.148-0.163 nm^3.

The crystallite size (D_{hkl}) was calculated using the Scherrer equation and the mean size (D) by the Williason-Hall "SSP" method, those reached lower values than other LDHs synthesized by coprecipitation, but those were similar to the LDHs obtained by the sol-gel technique [Ni/Al-CO$_3^{2-}$] ($2.69 \leq D_{003} \leq 8.11$ nm) [38,45,46].

Analysis of batch settling test

Batch settling tests at initial solids concentration ranging from 94 to 168 kg m^{-3}, density of the slurry (ρ_p) 971 to 1019 kg m^{-3} and temperature 53 ± 4 °C were carried out. The height of the interface between the settled solids and the clear supernatant liquor was plotted as a function of time at different solids contents in Figure 10.

Then, the free settling velocity (v_f / m h^{-1}), critical velocity (v_c / m h^{-1}) and the unit area of sedimentation (UA / m^2 day t^{-1}) were determined through the Talmadge and Fitch´s method.

As shown in Figure 11a, increasing the solids content from 120 to 168 kg m^{-3} decreased the free settling velocity to 0.22 m h^{-1} because increasing the concentration of particles suspended in a fluid increases the density and viscosity of the suspension, as well as collisions and interference between particles. Also, according to the Takacs´s equation, v_f decreased when the sludge concentration tended to zero. Similar behavior of the critical settling velocity was obtained (Figure 11b) [20,47,48].
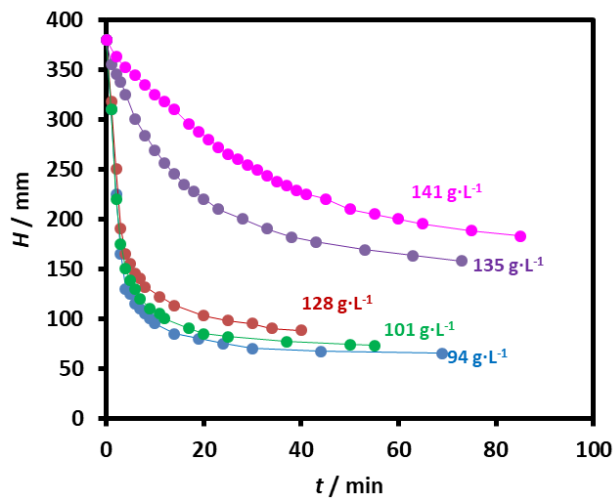
Figure 10. *Effect of solids content on settling curve (E-2)*

The unit area (UA / m^2 day t^{-1}) was obtained at different solids concentrations (Figure 11c). For the effluent liquor (E-2 and E-3), a tendency was observed to decrease the unit area with the increase in electric current density, which presupposes the formation of larger flocs.
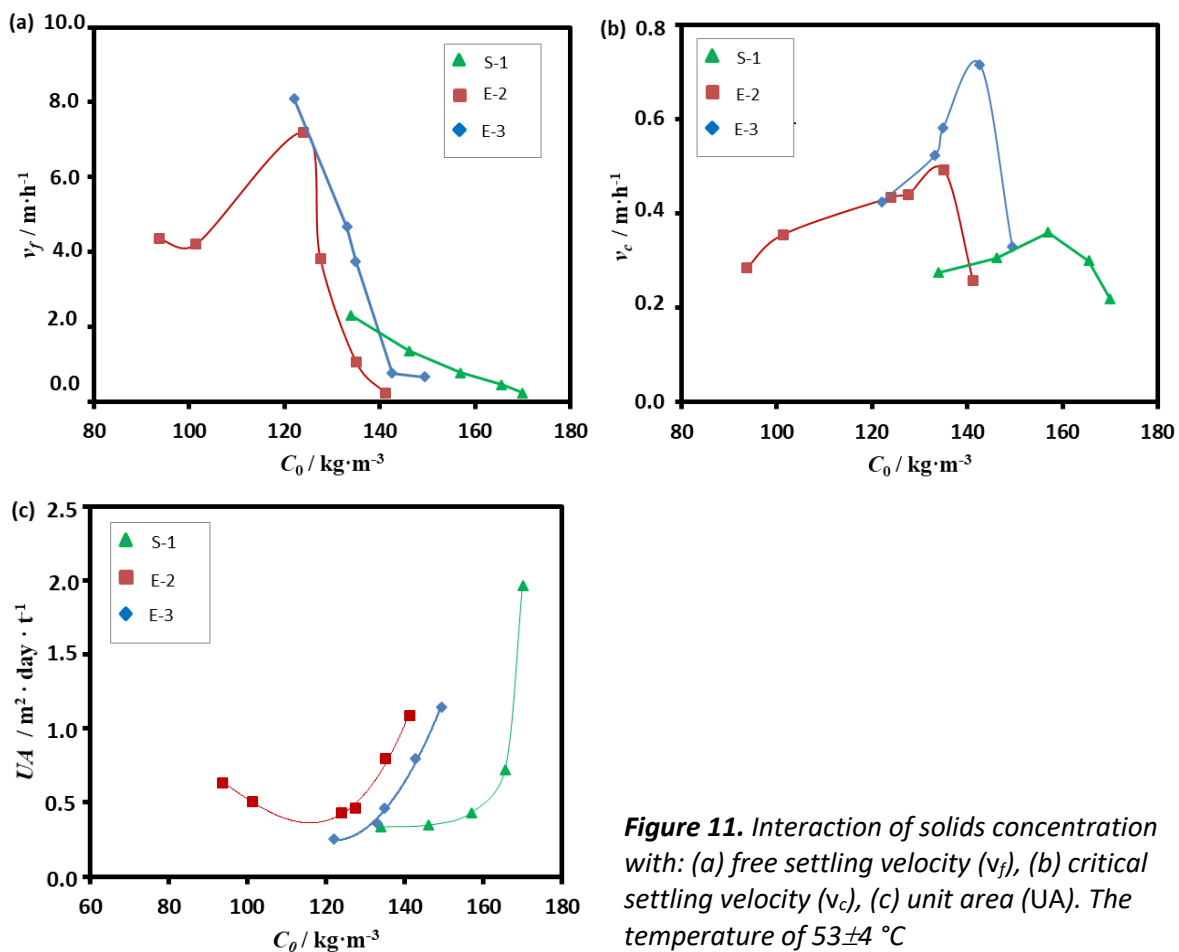

Figure 11. *Interaction of solids concentration with: (a) free settling velocity (v_f), (b) critical settling velocity (v_c), (c) unit area (UA). The temperature of 53$\pm$4 °C*

Furthermore, using the Coe and Clevenger´s formula, the unit area (UA), the settling velocity (v_s) and the suspended solids concentration (sp) were determined at 55 °C and different solids concentrations (C_0) (Table 7).

An increase in suspended solids was observed with increasing settling velocity and dilution of the suspension (Table 7), and the process possibly requires feeding flocculants. At a current density of 15.7 mA cm^{-2} suspended solids were not obtained.

Table 7. Results of settling tests by Coe and Clevenger´s formula (S-1)

		v_s / m h^{-1}	0.60	0.90	1.20	1.50	1.56
	128	UA / m^2 day t^{-1}	0.338	0.261	0.198	0.167	0.122
C_0 / kg m^{-3}		sp / mg L^{-1}	31	39	40	40	44
		v_s / m h^{-1}	0.60	0.90	1.20	1.50	1.68
	109	UA / m^2 day t^{-1}	0.308	0.236	0.173	0.102	0.099
		sp / mg L^{-1}	27	62	83	101	111

The density at 24 hours was 1065±20 kg m^{-3}, for a liquid-solid ratio 3.52±0.52 kg kg^{-1} and fraction by weight of solids 0.224±0.025 kg kg^{-1}, the pulp is not compact and easily detached from the test tube.

Analysis of the filtration and dye

The filtration resistances were determined at 60 °C for the method of constant pressure. The suspension density was 1015±11 kg m^{-3}, pH 8.69±0.10 and the cake density 1063±3 kg m^{-3}.

In all the experiments, the filtered volume (*V*) *vs.* time (*t*) followed a potential function (Figure 12a), and the general filtration equation for constant pressure in the plot of $t\,V^{-1}$ *vs.* V (Figure 12b) followed a linear function with high quality of fit, which is an indicator of goodness of fit for the observations. To the values of the independent variables planned, the specific cake resistance resulted in 10.56±5.94 ×10^7 m kg^{-1} and the filter medium resistance 1.62±0.96 ×10^8 kg^{-1}.
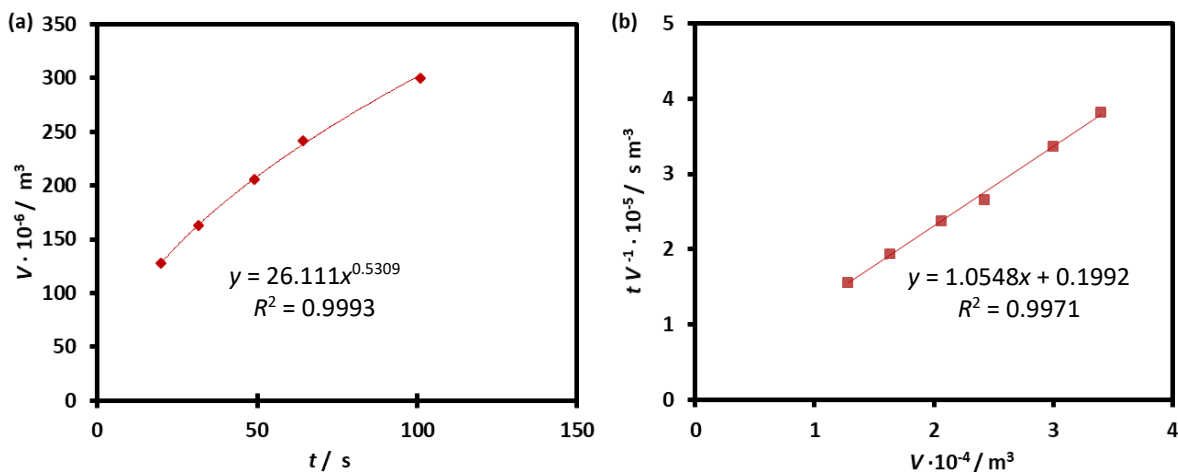

Figure 12. *Filtration at 44.45 kPa and C$_s$ 59.52 kg m^{-3} (E-2): (a) volume of filtrate versus time; (b) filtration general model adjustment*

A model was obtained to predict the specific cake resistance as a function of pressure drop between 27.7 and 44.4 kPa and suspension concentration of 25.0 to 60.4 kg solid per m^3 pure liquid. At a pressure drop 44.45 kPa and C_s 59.52 kg m^{-3}, the specific cake resistance resulted in 6.47±0.09×10^7 m kg^{-1}, eq. (25).

$$\alpha = 1.329\times10^6\,(\Delta P)^{2.95069}\,C_s^{-1.80727} \tag{25}$$

The coefficient of determination R^2 was 99.34 % and Adjusted R^2 99.16 %, which refers to the goodness of fit of a model. The cake humidity was 89±0.8 % humid base (Y_h).

Conclusions

The maximum nickel removal by electrocoagulation of the Ni(II)-NH$_3$-SO$_2$-CO$_2$-H$_2$O system was 99.7 % at 11.0 mA cm^{-2} with effluent liquor, the specific energy consumption 16.86 kWh per kg Al^{3+}, 2.438 kWh kg^{-1} of precipitated Ni and the adsorption capacity 5819 mg Ni per g Al^{3+}.

The electric current diminished by approximately 10 % with the reaction time, and the voltage increased a 15 % due to the formation of deposits on the electrode's surface and the removal of ionic species from de liquor. A greater area of electrodes, a lower voltage is required to generate the operating current.

The kinetic analysis suggested that the process is determined by the simultaneous contribution of the resistance: external diffusion, nucleation, the control of the chemical reaction and a possible autocatalytic effect.

The synthesis product had a nickel concentration of 37.2 %, cobalt 0.059 %, magnesium 1.3 %, aluminum 6.6 %, true density of 2720 kg m^{-3} and apparent density 640 kg m^{-3}, hydrotalcite-like structure layered double hydroxides, and phases impurities nickel oxide hydroxide, nickel aluminum oxide hydrate and aluminum oxide hydrate.

The unit area of sedimentation was between 0.252 and 1.965 m^2 t^{-1} day at a density of slurry from 971 to 1019 kg m^{-1} and a temperature of 53$\pm$4 °C. As the solids content increased, the free settling velocity and the critical settling velocity decreased and diminished when the sludge concentration tended to zero.

The specific cake resistance to filtration was proportional to the pressure drop and inversely proportional to the suspension concentration. A model was obtained to predict this resistance at 44.45 kPa and 59.52 kg solid per m^3 pure liquid, which resulted in 6.47$\times$10^7 m kg^{-1}. Finally, the average cake humidity was 88 %.

References

[1]   A. R. Vargas, M. E. M. Haynes, *Acta Chimica Slovenica* **67** (2020) 1239-1249. http://dx.doi.org/10.17344/acsi.2020.6147

[2]   A. R. Vargas, M. E. M. Haynes, A. R. Riverón, *Revista de Metalurgia* **55** (2019) e149. https://doi.org/10.3989/revmetalm.149

[3]   M. E. M. Haynes, A. R. Vargas, *Revista Tecnología Química* **33** (2013) 200-205. https://tecnologiaquimica.uo.edu.cu/index.php/tq/article/view/401

[4]   M. E. M. Haynes, *Revista Tecnología Química* **36** (2016) 27-36. https://tecnologiaquimica.uo.edu.cu/index.php/tq/article/view/595

[5]   S. R. Rivas, G. M. Vuelta, R. A. Rodríguez, *Revista Tecnología Química* **36** (2016) 145-153. https://tecnologiaquimica.uo.edu.cu/index.php/tq/article/view/1118

[6]   A. R. Vargas, A.R. Riverón, M. P. Medina, *Revista Tecnología Química* **40** (2020) 363-382. https://tecnologiaquimica.uo.edu.cu/index.php/tq/article/view/5155

[7]   F. Y. AlJaberi, S. A. Ahmed, H. F. Makki, *Heliyon* **6** (2020) e03988. https://doi.org/10.1016/j.heliyon.2020.e03988

[8]   F. Y. AlJaberi, *Chemical Engineering and Processing - Process Intensification* **174** (2022) 108864. https://doi.org/10.1016/j.cep.2022.108864

[9]   N. Beyazit, *International Journal of Electrochemical Science* **9** (2014) 4315- 4330.

[10]   P. T. Sabedot, E. B. Jonko, *Korean Journal of Chemical Engineering* **34** (2017) 2631-2640. https://doi.org/10.1007/s11814-017-0178-y

[11]   S. Zhang, X. Yang, Q. Cheng, M. Wang, C. Hu, B. Chai, J. Li, *Environmental Engineering Science* **35** (2018) 861-871. https://doi.org/10.1089/ees.2016.0621

[12]   A. R. Vargas, A.R. Riverón, M. E. M. Haynes, D. D Álvarez, S. C. Sánchez, *Revista Tecnología Química* **42** (2022) 114-130. https://tecnologiaquimica.uo.edu.cu/index.php/tq/article/view/5227

[13]   H. S. Coe, G. H. Clevenger, *Trans AIME* **55** (1916) 356-385.

[14]   G. J. Kynch, *Transactions of the Faraday Society* **48** (1952) 166-175. https://doi.org/10.1039/TF9524800166

[15]   W. P. Talmadge, E. B. Fitch, *Industrial & Engineering Chemistry* **47** (1955) 38-41. https://doi.org/10.1021/ie50541a022

[16]   J.H. Wilhelm, Y. Naide, *Soc. Min. Eng. AIME annual meeting. New Orleans*, 1979, Preprint N 79-30, p. 18.

[17]   C. C. Obunwo, S.D. Iboroma, A.P. Bagshaw, *Journal of Applied Science and Environmental Management* **21** (2017) 307-311. https://dx.doi.org/10.4314/jasem.v21i2.11

[18]   S.l. Xu, S. Rui, Y.Q. Cai, H.L. Sun, *Granular Matter* **20** (2018) 1-17. https://doi.org/10.1007/s10035-017-0769-7.

[19]   J. Zhang, W. Zhou, J. Liang, Q. Zhang, *Effects of Temperature on the Flocculation Processes of Kaolinite in the Quiescent Water, International Conference on Asian and Pacific Coasts (APAC 2019)*, Singapore, 2020. https://doi.org/10.1007/978-981-15-0291-0_71

[20]   A. H. Ghawi, J. Kriš, *Study the effect of temperature on rectangular sedimentation tanks performance, XX-TH Jubilee-National, VIII-TH International Scientific and Technical Conference Water Supply and Water Quality*, Poland, 2008, p. 440.

[21]   Z. Potok, T. Rogozinski, *Sustainability* **12** (2020) 4816. https://doi.org/10.3390/su12124816

[22]   F. M. Mahdi, T. N. Hunter, R. G. Holdich, *Processes* **7** (2019) 746. https://doi.org/10.3390/pr7100746

[23]   O. J. Ituma, A. Joel, *International Journal of Scientific & Engineering Research* **9** (2018), 2222-2232.

[24]   N. S. Zafisaha, W. L. Ang, A. W. Mohammada, N. Hilalc, *International Journal of Engineering, Transactions B* **31** (2018) 1437-1445. https://doi.org/10.5829/ije.2018.31.08b.36

[25]   A. R. Cestari, E. F. S. Vieira, G. S. Vieira, *Journal of Hazardous Materials* B138 (2006) 133–141. https://doi.org/10.1016/j.jhazmat.2006.05.046.

[26]   E. F. S. Vieira, A. R. Cestari, E. C. N. Lopes, *Reactive & Functional Polymers* **67** (2007) 820–827. https://doi.org/10.1016/j.reactfunctpolym.2006.12.005

[27]   B. Royer, N. F. Cardoso, E. C. Lima, T. R. Macedo, C. Airoldo, *Separation Science and Technology*, **45** (2010) 129-141. http://dx.doi.org/10.1080/01496390903256257

[28]   E. C. Lima, A. R. Cestari, M. A. Adebayo, *Desalination and Water Treatment*, **57** (2016) 19566-19571. https://doi.org/10.1080/19443994.2015.1095129

[29]   A. I. Adeogun, R. B. Balakrishnan, *Applied Water Science* **7** (2017) 1711-1723. https://doi.org/10.1007/s13201-015-0337-4

[30]   A. A. Inyinbor, F. A. Adekola, G. A. Olatunji, *Water Resources and Industry* **15** (2016) 14–27. http://dx.doi.org/10.1016/j.wri.2016.06.001

[31]   H.N. Tran, S.-J. You, A. Hosseini-Bandegharaei, H.-P. Chao, *Water Research* **120** (2017), 88-116. https://doi.org/10.1016/j.watres.2017.04.014

[32]   N. Ç. Selçuk, Ş. Kubilay, A. Savran, A. R. Kul, *Journal of Applied Chemistry* **10** (2017) 53-63. https://doi.org/10.9790/5736-1005015363

[33]   L. W. Arimieari, J. O. Ademiluyi, *Journal of Environmental Protection* **9(2)** (2018) 91-99. https://doi.org/10.4236/jep.2018.92007

[34]   J. R. O. Gutiérrez, A. V. Rojas, *Revista Tecnología Química,* **38** (2018) 24-35. https://tecnologiaquimica.uo.edu.cu/index.php/tq/article/view/3213

[35]   D. Marmanis, K. Dermentzis, A. Christoforidis, V. Diamantisb, K. Ouzounisb, A. Agapiouc, M. Stylianou, *Journal of Power Technologies* **98** (2018) 377–381. https://papers.itc.pw.edu.pl/index.php/JPT/article/view/1462

[36]   N. A. Oladoja, *Desalination and Water Treatment* **57** (2016) 15813-15825. http://dx.doi.org/10.1080/19443994.2015.1076355

[37]   Y. Zhao, F. Xiao, Q. Jiao, Journal of Nanotechnology 2011 (2011) 646409. http://dx.doi.org/10.1155/2011/646409

[38]   M. Jitianu, D. C. Gunness, D. E. Aboagye, M. Zaharescu, A. Jitianu, Materials Research Bulletin 48 (2013) 1864-1873. http://dx.doi.org/10.1016/j.materresbull.2013.01.030

[39]   S. Jaerger, S. F. Zawadzki, A. Leuteritzb, F. Wypych, *Journal of the Brazilian Chemical Society* **28** (2017) 2391-2401. http://dx.doi.org/10.21577/0103-5053.20170093

[40]   B. Habibi, S. Ghaderi. *Electrosynthesized, Bulletin of Chemical Reaction Engineering & Catalysis* **12** (2017) 1-13. http://dx.doi.org/10.9767/bcrec.12.1.460.1-13

[41]   W. M. A. El Rouby, S. I. El-Dek, M. E. Goher, S. G. Noaemy, *Environmental Science and Pollution Research* **27** (2020) 18985-19003. https://doi.org/10.1007/s11356-018-3257-7

[42]   M. Rajamathi, P. V. Kamath, *Bulletin of Materials Science* **23** (2000) 355–359. https://doi.org/10.1007/BF02708384

[43]   F. Z. Mahjoubi, A. Khalidi, O. Cherkaoui, R. Elmoubarki, M. Abdennouri, N. Barka, *Journal of Water Reuse and Desalination* **7** (2017) 307-318. https://doi.org/10.2166/wrd.2016.041

[44]   F. Z. Mahjoubi, A. Elhalil, R. Elmoubarki, M. Sadiq, A. Khalidi, O. Cherkaoui, N. Barka, *Journal of Applied Surfaces and Interfaces* **2(1-3)** (2017) 1-11. https://doi.org/10.48442/IMIST.PRSM/jasi-v2i1-3.10033

[45]   L. Yang, Z. Liu, S. Zhu, L. Feng, W. Xing, *Materials Today Physics* **16** (2021) 100292. https://doi.org/10.1016/j.mtphys.2020.100292

[46]   Y. T. Prabhu, K. V. Rao, V. S. Kumar, B. S. Kumari, *World Journal of Nano Science and Engineering* **4** (2014) 21-28. http://dx.doi.org/10.4236/wjnse.2014.41004

[47]   I. Takacs, G. Patry, D. Nolasco, *Water Research* **25** (1991) 1263-1271. https://doi.org/10.1016/0043-1354(91)90066-Y

[48]   P. Balbierz, K. Rucka, *Sludge settling characterization for the mathematical modelling of sidestream treatment processes*, *9th Conference on Interdisciplinary Problems in Environmental Protection and Engineering (EKO-DOK), E3S Web of Conferences* **17** (2017) 00003. https://doi.org/10.1051/e3sconf/20171700003